Journal of Alloys and Compounds 541 (2012) 495–504

Contents lists available at SciVerse ScienceDirect

Journal of Alloys and Compounds

journal homepage: www.elsevier.com/locate/jalcom

Effects of thickness and atmospheric annealing on structural, electrical and optical properties of GZO thin films by spray pyrolysis

T. Prasada Rao [a,b,*], M.C. Santhosh Kumar [a], N. Sooraj Hussain [b]

[a] Advanced Materials Laboratory, Department of Physics, National Institute of Technology, Tiruchirappalli 620 015, India
[b] INESC Porto/Department of Physics, University of Porto, 4169-007 Porto, Portugal

ARTICLE INFO

Article history:
Received 26 December 2011
Received in revised form 28 May 2012
Accepted 31 May 2012
Available online 6 July 2012

Keywords:
Thin films
Chemisorption
Electrical properties
Optical properties

ABSTRACT

Gallium doped zinc oxide (GZO) films have been prepared on glass substrates by the spray pyrolysis (SP) technique. The effects of thickness and annealing in air and oxygen on structural, electrical and optical properties of GZO thin films were investigated. As-deposited films were found polycrystalline with hexagonal structure that showed compressive stress along the *c*-axis. The compressive stress was found to decrease by thickness and by annealing in air or oxygen. The best characteristics have been obtained after heat treatment in oxygen, where the highest carrier concentrations have been achieved and with visible transmittance of 85–70% and resistivity of $4.21–2.25 \times 10^{-3}$ Ωcm with increasing thickness. The band gaps of oxygen annealed samples are found to have low values in comparison to air annealed and as deposited samples. The band gap dependence on the film thickness and annealing atmosphere is correlated to the shrinkage effect. Photoluminescence (PL) study was confirmed that broad visible emission in GZO films due to both the intrinsic traps and deep level vacancies.

1. Introduction

The ZnO semiconductor has attracted much attention because of its wide applications for various optoelectronic devices. The notable properties of ZnO are its direct band gap of 3.37 eV at room temperature and high exciton bonding energy 60 meV which is higher than the values of GaN (21 meV) and ZnSe (20 meV) [1].Transparent conducting oxides (TCOs) including SnO_2:F, ZnO:Al, and In_2O_3:Sn (ITO) have attracted considerable attention due to their great potential in photoelectric applications [2]. In addition, the use of TCO materials for specialized applications requires consideration of various factors such as cost and toxicity of materials, stability of various properties in thin films and suitability of film deposition [3]. Gallium is an effective *n*-type dopant in ZnO since the covalent bond length of Ga–O (1.92 Å) is nearly equal to that of Zn–O (1.97 Å). On the other hand, the Ga, Al and In doped ZnO nanostructures are believed to have more potential for diverse applications [4]. By means of doping, large conductivities combined with large ranges of transparency in the visible (VIS) and near UV range can also be obtained [5,6]. The resistivity stability at high temperatures is successfully improved in transparent conducting ZnO films doped with a donor impurity such as Al or Ga [7,8]. The resistivity stability was considerably dependent on the film deposition conditions and content of doped impurity [9–13]. The resemblance in atomic radius (Ga, 0.062 nm and Zn, 0.083 nm) and bond lengths [14] result in less lattice deformation for Ga-doping during high temperature processing, even under higher doping level.

Implementation of the various functionalities requires customized methods of bulk and thin film growth, doping or alloying, metallization, and processing. A common component of almost any such process is heat treatment, and that used either during processing steps such as growth, doping, and alloying or used in a post-processing phase. Several studies have focused on the influence of postdeposition annealing on structural, morphological, electrical and optical properties of GZO thin films. In the present study, we have deposited transparent conducting gallium-doped zinc oxide (ZnO:Ga) films by spray pyrolysis (SP) and subsequently annealed for 30 min at 673 K, in oxygen and air. We have investigated the effect of film thickness and the effect of atmospheric heat treatment on the structural, morphological, optical and electrical properties of GZO thin films deposited by SP technique.

2. Experimental

Spray pyrolysis is an effective method for the deposition of thin films of metallic oxides, as is the case with the GZO material. The precursor solution for spray pyrolysis was prepared by dissolving an appropriate amount of zinc acetate dehydrate and gallium nitrate in the mixture of deionized water and ethanol at room temperature. In this mixture, ethanol concentration was 10 mL in 100 mL solution. A few

* Corresponding author at: Advanced Materials laboratory, Department of Physics, National Institute of Technology, Tiruchirappalli 620 015, India. Tel.: +91 9894569421; fax: +91 0431 2500133.
E-mail addresses: prasadphd2011@gmail.com (T. Prasada Rao), santhoshmc@nitt.edu (M.C. Santhosh Kumar).

0925-8388/$ - see front matter © 2012 Elsevier B.V. All rights reserved.
http://dx.doi.org/10.1016/j.jallcom.2012.05.128

drops of acetic acid were added to aqueous solutions to prevent the formation of hydroxides. The concentration of gallium was 3 at.%. The total concentration of the solution was maintained at 0.2 mol L^{-1}. The glass substrates were cleaned thoroughly with acetone, isopropanol and finally with deionized water with the help of an ultrasonic bath. The nozzle was at a distance of 20 cm from the substrate during deposition. The solution flow rate was held constant at 3 mL/min. Air was used as the carrier gas at the pressure of 2 bar. When aerosol droplets arrive nearer to the substrates, a pyrolytic process occurs and highly adherent GZO films were formed. The GZO thin films were deposited at substrate temperature of 623 K with different thickness. As-deposited samples were annealed in air and oxygen atmosphere at 673 K.

The thickness was measured using KLA-Tencor Alpha step IQ surface profiler. The structural properties were studied by X-ray diffraction measurements (XRD) using Rigaku D/Max ULTIMA III diffractometer with Cu Kα radiation (λ = 1.5406 Å). The average dimensions of crystallites were determined by the Scherer method from the broadening of the diffraction peaks. The surface chemical analysis was carried out by X-ray photoelectron spectroscopy (XPS) with anylizer PHOIBOS HSA3500 100 R4 [HWtype 30:2] MCD-5 instrument. Al Kα (1486.61 eV) radiation was used as the excitation source. The surface morphology profiles of the samples were recorded using Nanoscope-E instrument with NSE -287 controllers. Fluorolog-3 spectroflurometer with 450 W xenon arc lam was used for PL study. Electrical properties namely, resistivity, Hall mobility, and carrier concentration were measured at room temperature using an Ecopia Hall measurement system (Model: HMS-3000) in van der Pauw configuration. The film composition of the GZO was determined using energy dispersive X-ray analysis (EDX, JEOL Model JED-2300) attached with SEM (BJEOL Model JSM-6390LV).

3. Results and discussion

3.1. Structural properties

We have investigated the changes in structural characteristics such as the crystal structure and surface morphology by means of XRD and AFM, to explore the dependence of structural properties on the thickness and annealing atmosphere. Fig. 1 shows the XRD spectra obtained for the as deposited, air annealed and oxygen annealed films with different thickness, respectively. It is seen that most dominant peaks are due to ZnO (002) planes, indicating that GZO films have polycrystalline nature with the textured growth along the *c*-axis. The c axis orientation in ZnO:Ga films can be understood by the "survival of the fastest" model proposed by Drift [15]. According to this model, nucleations with various orientations can be formed at the initial stage of the deposition and each nucleus competes to grow but only nuclei having the fastest growth rate can survive, i.e., *c*-axis orientation is achieved. Also, the (002) orientated grains have the lowest surface energy [16]. The diffraction peaks are easily indexed on the basis of the hexagonal structure of ZnO (a = 3.242 Å, and c = 5.194 Å, JCPDS 75-0576). The intensity of the GZO peaks increases with the film thickness. This indicates that as the film thickness increases the crystallinity of the films improves. No metallic Ga or gallium oxide characteristic peaks are observed in the diffraction patterns, which implies that gallium atoms replace zinc in the hexagonal lattice and/or gallium segregate to the non-crystalline region in grain boundary. This means that the single phase of ZnO has been obtained for all samples with the same spraying conditions. The (002) peaks showed a deviation from 2θ = 34.50° (value for ZnO powder, JCPDS 75-0576). The diffraction angle of the peaks is gradually shifted towards 34.50° with increasing film thickness. A larger deviation was observed for as deposited ZnO films and those doped with Ga. These deviations indicate that the interplanar spacing changed relative to that of the ZnO powder, which is probably due to factors such as lattice strain and interstitial defects [17]. There is a notable increase in the intensity of (002) peak for the annealed samples in air and oxygen. Comparatively, high intensity of XRD peaks implies that the crystalline quality is better for GZO film annealed in oxygen ambient. Scherer's formula was employed to estimate the crystal size of GZO films, given by

$$D = \frac{0.9\lambda}{\beta \cos\theta} \tag{1}$$

where D is the average dimension of the crystallites normal to the reflecting planes, β is the crystallite-size breadth defined by $\beta^2 = B^2 - b^2$ in which B is the FWHM of observed peak, b is the instrumental factor. From the Table 1, it can be seen that the grain sizes did not change significantly with increasing film thickness. There is slight increase in the grain size after annealing in air and oxygen (Table 1). The grain boundary is one of the primary factors influencing the electrical properties of thin films. In this regard, changing grain sizes imply that grain size effect would also be relatively significant in the interpretation of the measured electrical properties of these GZO films. Therefore, any change in electrical and optical properties could be mainly correlated to the thickness and the processing history (air and oxygen annealing). The lattice constant '*c*' was calculated for (002) plane using the following equation [18]:

$$\frac{1}{d^2_{(hkl)}} = \frac{4}{3}\left[\frac{h^2 + hk + k^2}{a^2}\right] + \frac{l^2}{c^2} \tag{2}$$

The average uniform strain ε_{zz} in the lattice along the *c*-axis of the ZnO films annealed at different temperatures have been estimated from the lattice parameters using the following expression [18]:

$$\varepsilon_{zz} = \frac{(c - c_0)}{c_0} \times 100\% \tag{3}$$

where c is the lattice parameter of the strained ZnO films calculated from X-ray diffraction data and c_0 is the unstrained lattice parameter of ZnO. The residual stress in the films is composed of thermal stress and intrinsic stress, the former comes from the difference in the thermal expansion coefficients between the coating and the substrate, while the latter originates from the ingrown defects or structural mismatch between the film and substrate [19]. In this study, the dependence of total residual stress on the thickness and annealing ambient was investigated, with the assumption that thermal stress is a constant due to the same deposition temperature. For hexagonal crystals, the stress (σ) in the plane of the film can be calculated using the biaxial strain model [20]:

$$\sigma_{film} = \frac{2C_{13}^2 - C_{33}(C_{11} + C_{12})}{C_{13}} \cdot \varepsilon_{zz} \tag{4}$$

where C_{11} = 209.7 GPa, C_{12} = 121.1 GPa, C_{13} = 105.1 GPa, and C_{33} = 210.9 GPa are the elastic stiffness constants of bulk ZnO. From the Table 2, the value of σ is negative, demonstrating that the stresses in the deposited films are compressive in the direction of the *c*-axis. It is well known fact that defects in the films are formed during the growth process. These defects cause lattice disorder, which generates the intrinsic stress in the films. As can be seen, in general, the values of the strain and the stress decrease with increasing film thickness. The stress and stain are higher in the as deposited GZO films. Obviously the presence of the doping atoms Ga causes an increase in the lattice disorder of the ZnO films. An additional decrease in the strain and stress is observed in all the films after oxygen annealing. This result is a consequence of the decrease in oxygen vacancies during the annealing process in oxygen.

Fig. 2 shows the AFM images of as deposited GZO thin films with different thickness and annealed at a temperature of 673 K in air and oxygen. The images are obtained in contact mode taken over a scale of 1 × 1 μm^2. The results of the grain size calculated by the Debye–Scherrer formula as well as by AFM are presented in Table 1. With increase in the thickness of the film the grains grow in size and are found to be uniformly distributed. When the deposition begins, there are many nucleation centers formed on the substrate and small crystallites are produced. The films are deposited for only a short time, the small crystallites on the substrate are not able to grow into large crystallites, and therefore the thinner films have smaller crystallites than the thicker films [21]. With

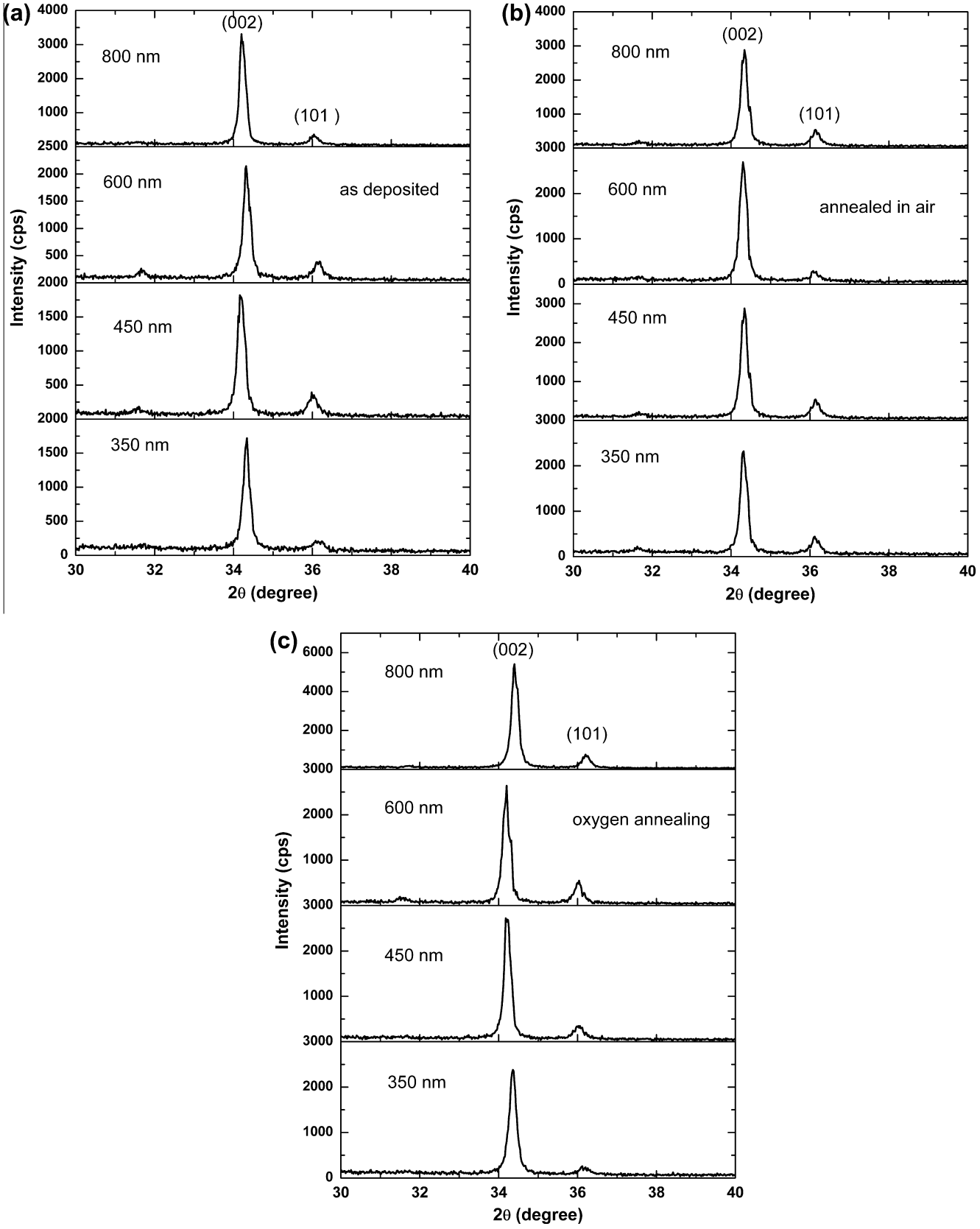

Fig. 1. XRD patterns of GZO thin films with various thicknesses (a) as deposited, (b) annealed in air, (c) annealed in oxygen.

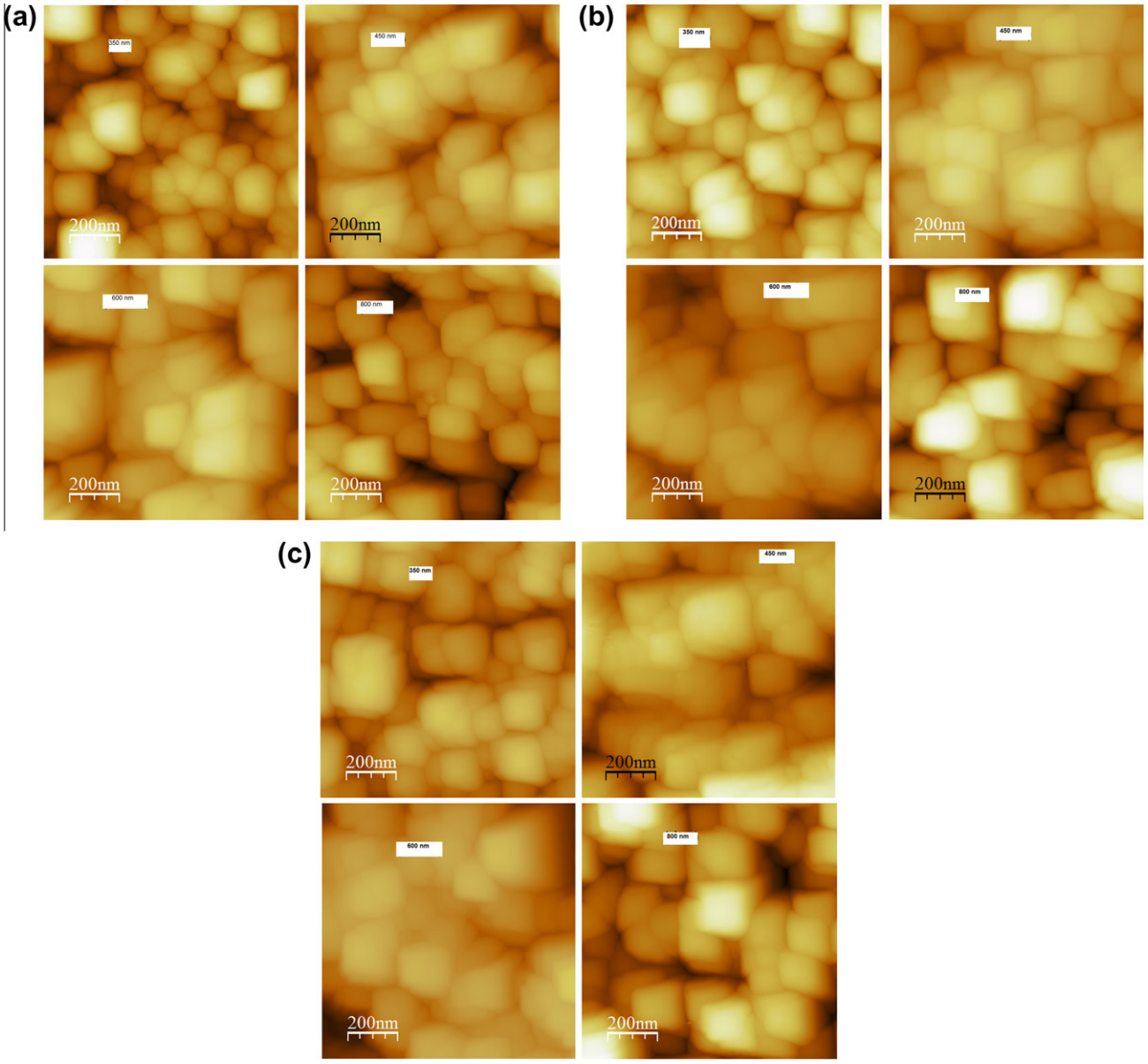

Fig. 2. AFM micrographs of GZO thin films with various thicknesses (a) as deposited, (b) annealed in air, (c) annealed in oxygen.

Table 1
Particle size and roughness (r.m.s value) values of as deposited, annealed samples with various thicknesses.

Thickness (nm)	As prepared			Annealed in air			Annealed in oxygen		
	Grain Size (nm) XRD	Particle size (nm) AFM	Roughness (nm)	Grain Size (nm) XRD	Particle size (nm) AFM	Roughness (nm)	Grain Size (nm) XRD	Particle size (nm) AFM	Roughness (nm)
350	43.5	159.5	19.0	44.8	173.6	27.0	44.0	165.3	18.0
450	44.0	162.0	32.3	46.0	185.7	44.0	46.4	194.1	37.6
600	46.3	169.0	38.2	47.6	196	49.7	48.0	202.0	48.0
800	48.1	178.4	46.7	49.8	211.5	58.1	49.3	219.8	55.7

increasing film thickness, the crystallinity of the films have been improved and the crystallite sizes become larger. This result is consistent with the XRD observation. After annealing, the surface roughness of GZO films increased. However, the films annealed in oxygen showed lower surface roughness than that in air.

The surface composition of films with thickness 350 nm was determined using XPS technique. The XPS spectra of the GZO films (Fig. 3) show that the binding energy (BE) of each constituent element is positioned at 1117.72 eV ($Ga2p_{3/2}$), 1022.23 eV ($Zn2p_{3/2}$) and 530.9 eV (O1s) respectively as calibrated to 285.43 eV (C1s). The binding energy of $Ga2p_{3/2}$ is shown in Fig. 4. The broadening of oxygen spectrum (Fig. 5) is believed to be composed of two components located at around 531 eV and 532 eV respectively. The low BE component is ascribed to covalently bonded oxygen in ZnO

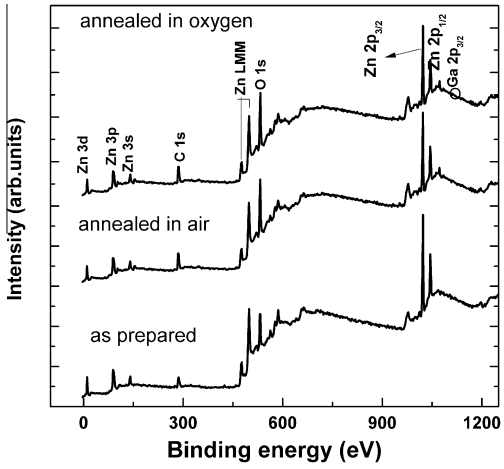

Fig. 3. XPS survey spectra of GZO thin films with 350 nm thickness.

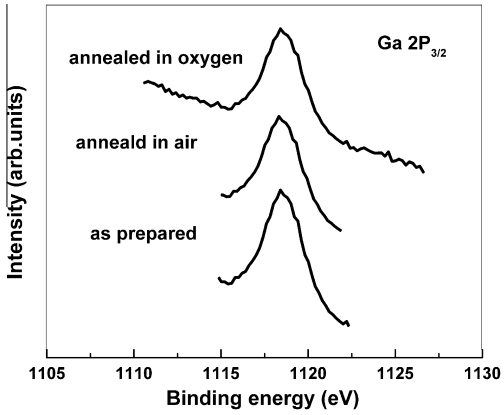

Fig. 4. Ga $2p_{3/2}$ spectra of GZO thin films with 350 nm thickness.

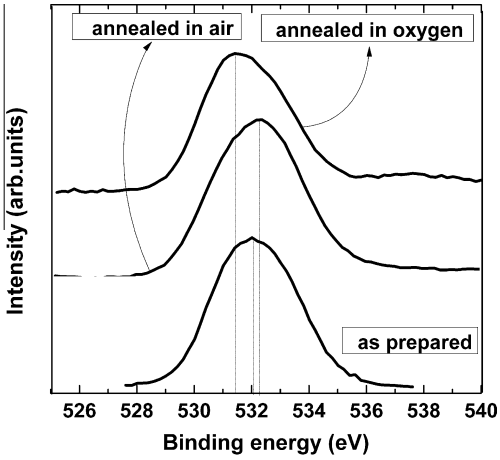

Fig. 5. Oxygen (O1s) spectra of GZO thin films with 350 nm thickness.

structure (lattice oxygen) while the high BE is attributed to the adsorbed oxygen [22–24]. The higher binding energy at 532 eV is usually attributed to chemisorbed or dissociated oxygen or OH species on the surface of the ZnO thin film [25,26]. Binding energy of O1s of as prepared, air annealed and oxygen annealed are 532.05, 532.33 and 531.43 eV respectively. The binding energy of O1s is high when heat treatment carried out in air. This O1s peak at binding energy of 532.33 eV is clearly indicating the presence of chemisorbed oxygen in the samples. During annealing in oxygen ambient, oxygen vacancies are complemented dominantly by chemisorption process and this combines with sufficient Zn atoms to form a new ZnO [27], resulting in the decrease of oxygen chemisorption i.e. decrease in oxygen binding energy. The increase of binding energy for sample annealed in air is mainly because of low oxygen absorption during annealing (oxygen not sufficient to form a new ZnO). It is well consistent with observation of O1s peaks for annealed films in different ambients. This result indicates the stoichiometry and structure of GZO thin film annealed in oxygen is better than that of annealed in air. The film composition of the as deposited GZO film with thickness 800 nm was determined using energy dispersive X-ray analysis (EDX). The average atomic percentage (at.%) of zinc, oxygen and gallium was 63.10, 34.56 and 2.34, respectively.

3.2. Electrical studies

Table 3 shows resistivity (ρ), carrier concentration (n) and Hall mobility (μ) as function of film thickness, before and after annealing in air and oxygen for GZO films. The carrier concentration and mobility increases when the film thickness varies from 350 to

Table 2
Lattice parameter, strain and stress of as deposited, annealed samples with various thicknesses.

Thickness (nm)	As prepared				Annealed in air				Annealed in oxygen			
	2θ (°)	c (Å)	Strain (%)	Stress (GPa)	2θ (°)	c (Å)	Strain (%)	Stress (GPa)	2θ (°)	c (Å)	Strain (%)	Stress (GPa)
350	34.30	5.224	0.57	−2.61	34.32	5.220	0.50	−2.27	34.35	5.217	0.44	−2.00
450	34.32	5.221	0.51	−2.35	34.33	5.220	0.50	−2.27	34.40	5.209	0.28	−1.30
600	34.35	5.217	0.44	−2.00	34.41	5.208	0.26	−1.22	34.44	5.204	0.19	−0.87
800	34.40	5.209	0.28	−1.30	34.45	5.202	0.15	−0.69	34.49	5.196	0.03	−0.17

Table 3
Resistivity, carrier concentration and mobility of as deposited, annealed samples with various thicknesses.

Thickness (nm)	As prepared			Annealed in air			Annealed in oxygen		
	$\rho \times 10^{-3}\ \Omega$ cm	$n \times 10^{19}$ cm^{-3}	μ cm^2/Vs	$\rho \times 10^{-3}\ \Omega$ cm	$n \times 10^{19}$ cm^{-3}	μ cm^2/Vs	$\rho \times 10^{-3}\ \Omega$ cm	$n \times 10^{19}$ cm^{-3}	μ cm^2/Vs
350	5.00	6.58	18.99	7.14	4.62	18.94	4.21	6.70	22.15
450	4.10	6.90	22.09	6.12	5.10	20.02	3.20	7.32	26.68
600	3.51	7.62	23.36	5.42	6.00	19.21	2.72	8.62	26.65
800	2.93	9.10	23.40	4.13	7.61	19.88	2.25	9.88	28.11

800 nm. Accordingly, resistivity decreases from 5.00×10^{-3} to 2.93×10^{-3} Ωcm. In general, the electrical resistivity decreases, as the film thickness increases. This can be understood from grain size variation observed from the AFM images. As the grain size increases with the thickness; the scattering mechanisms in the grain boundaries are diminished by the reduction of the number of grain boundaries [28]. Additionally, from the XRD spectra it is evident that thicker films have a better crystallinity. As a result of the enhancement of structural characteristics with film thickness, the electrical properties are improved as well. The resistivity reduction with increase in film thickness is mainly attributed to reduction in grain boundary scattering. In the present case, ionized impurity scattering is insignificant because of low impurity doping (Ga 3 at.%).

After annealing all the samples in air, the resistivity markedly increased and carrier concentration decreased in comparison with as deposited samples. It is well known that in semiconductor thin films, free carriers may interact with all kind of atoms and defects in the lattice and grain boundary regions [29]. As a result, the free carriers are scattered and consequently the film resistivity increases. It is primarily due to the decrease in carrier concentration, which is attributed to electron traps due to the chemisorbed oxygen onto the grain boundaries. Chemisorbed oxygen enhances the formation of trapping states. These trapping states are capable of trapping carriers and thereby immobilizing them. This reduced the number of free carriers available for electrical conduction. After trapping the mobile carriers, the traps became electrically charged, creating a potential energy barrier which impeded the motion of carriers from one crystallite to another, thereby reducing their mobility [30]. According to Tansley et al. [31] the presence of ionized adsorbates on the crystalline surfaces could increase the intercrystalline barrier height, which decreases the effective carrier mobility and hence the conductivity. It was noted that the carrier mobility of GZO film annealed in air was controlled by the intercrystalline depletion barriers. In the case of oxygen annealed samples, the electrical properties marginally improved in comparison with as deposited and air annealed samples. This improvement is mainly attributed to the reduction in chemisorbed oxygen at grain boundaries and enhancement in structural properties.

3.3. Optical properties

Fig. 6 shows the transmittance in the UV–Vis–NIR regions of ZnO:Ga films before and after annealing in air and oxygen with various thicknesses. It can be seen that the films are transparent to the visible light. It is observed that the average transmittance

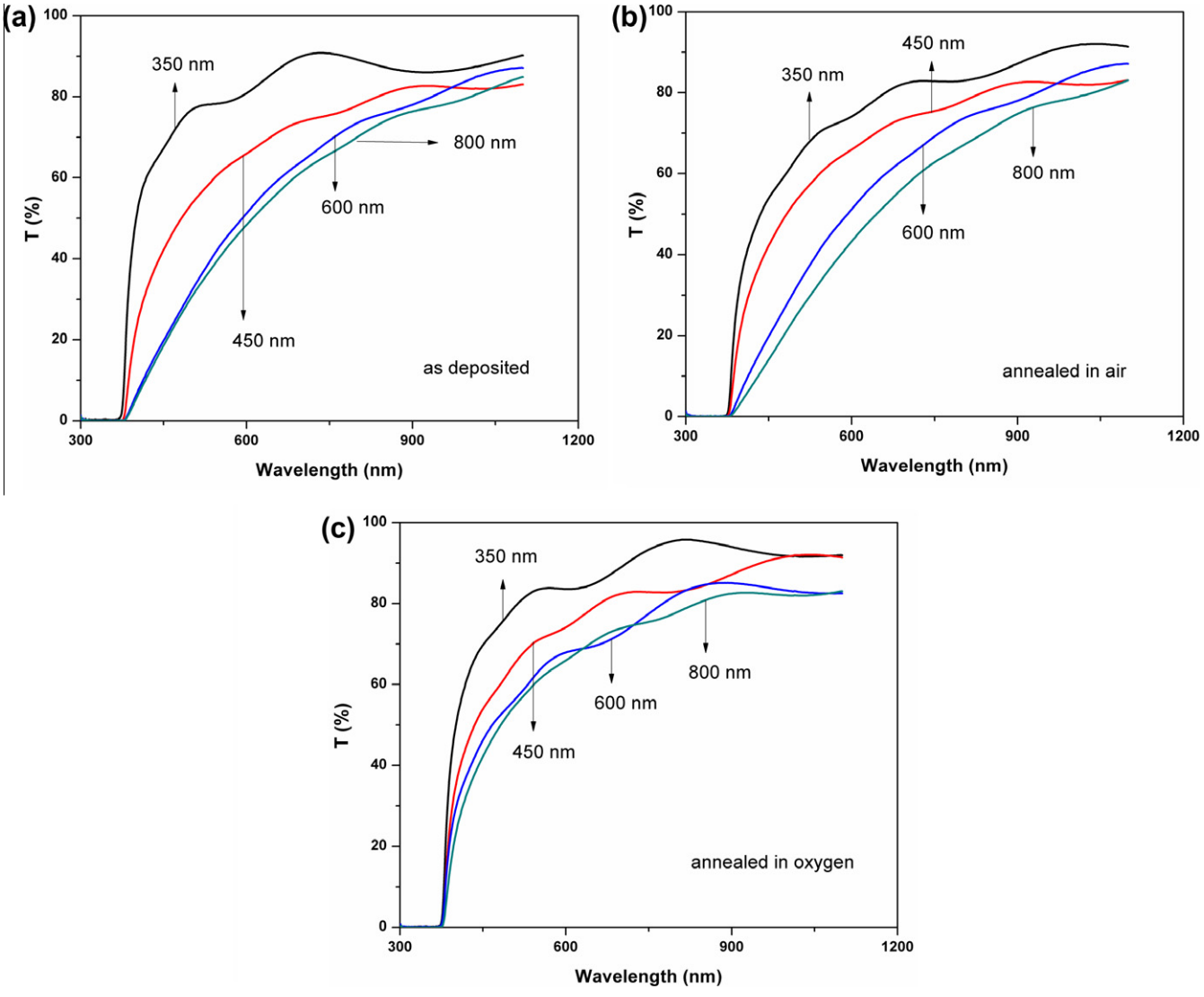

Fig. 6. Transmittance spectra of GZO thin films.

is about 80% in the visible region with 350 nm film thickness. It can be seen that the transmittance of the films decreases with increasing film thickness. It is also clear that the transmittance is improved by the oxygen heat treatment. It is well known that annealing TCO films in oxygen atmosphere improves their transmittance. A slight decrease in average transmission is observed in the sample annealed in air and is attributed to increase of surface roughness, which is evident from the AFM result. The optical transmittance of a film is known to depend strongly on its surface morphology. It could be observed that the transmission in the visible region decreased substantially at shorter wavelengths near the ultraviolet range for all films. The absorption coefficient α is calculated from the relation [32]:

$$T = (1 - R)\exp(-\alpha t) \quad (5)$$

where T is the transmittance, R is the reflectance and t is the film thickness. As a direct band gap semiconductor, the optical band gap (E_g) and optical absorption coefficient (α) of GZO thin film are correlated by the following formula [33]:

$$\alpha h\upsilon = A\sqrt{h\upsilon - E_g} \quad (6)$$

where $h\upsilon$ is the photon energy, A is the proportional constant. Fig. 7 shows the plot of square of the product of absorption coefficient and photon energy versues photon energy for as prepared and annealed samples. The E_g values slightly decrease with the film thickness as shown in Table 4. In general, changes in the band gap energy of ZnO thin films have been related to variations in the mean crystallite size, the internal stress and/or the free carrier concentration [34–38]. Based on the optical characterization, it is observed that the film transparency and the E_g values depend on the annealing atmosphere. It reveals that the optical band gap of the GZO films decreases with increasing carrier concentration. It is a well-known fact that two competing phenomena affect the band-gap energy values with increasing donor density, mainly in heavily doped semiconductors [39]. The first phenomenon is related with a widening of the band-gap energies of semiconductors due to the band-filling effect, which is known as Burstein–Moss (B–M) effect [40]. It is known that the Fermi energy of degenerate GZO films with electron carrier concentration above 10^{20} cm^{-3} penetrates into the conduction band. According to the B–M effect, raising the Fermi level into the conduction band of a degenerate semiconductor leads to energy band broadening [41]. It is known that for highly n-doped materials the band gap enlarges with the increase of carrier concentration, owing to a blocking of the lowest states of the conduction band by excess electrons [37]. The second one affects the band gap of ZnO films with carrier concentrations higher than the Mott critical concentration ($\sim 5 \times 10^{18}$ cm^{-3}) because the electron–electron and electron–impurity interactions give rise to a shift in energy of the valence and conduction bands, leading to a reduction of the band

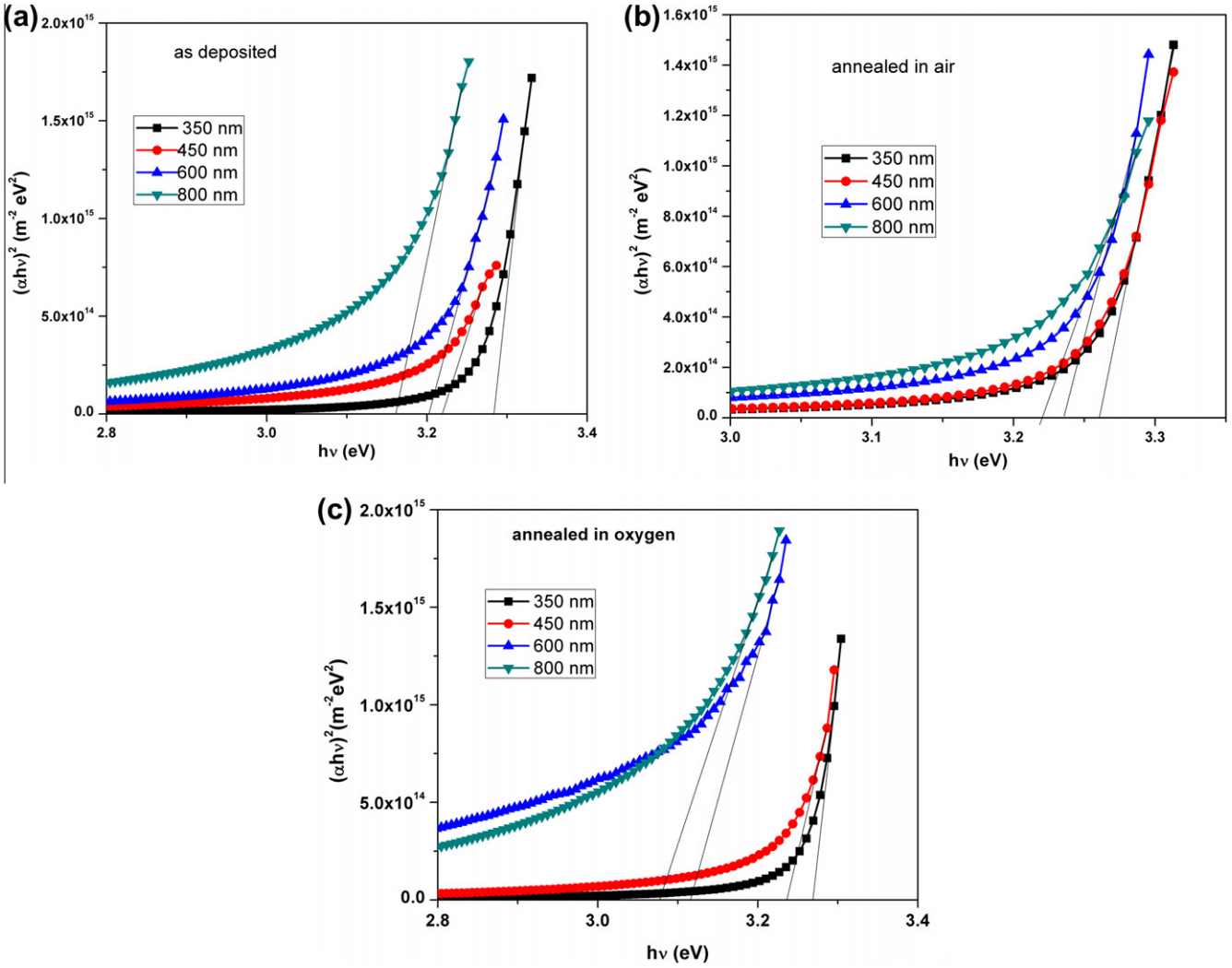

Fig. 7. $(\alpha h\upsilon)^2$ versus $h\upsilon$ spectra of GZO thin films.

Table 4
Optical energy band gap values of as deposited, annealed samples with various thicknesses.

Thickness (nm)	Energy band gap (eV)		
	As prepared	Annealed in air	Annealed in oxygen
350	3.28	3.26	3.26
450	3.22	3.26	3.23
600	3.20	3.23	3.11
800	3.16	3.22	3.07

gap[39]. However, our optical band gap results indicate that the B–M effect is weak. Therefore the shrinkage effect is dominant over the widening or B–M effect, since the E_g values decreases with the increase of film thickness. The band gap of all oxygen annealed samples is having low values in comparison with air annealed and as deposited samples, since carrier concentration is higher for oxygen annealed samples.

Photoluminescence (PL) is very sensitive to the quality of crystal structure and to the presence of defects. The band-to-band excitation of ZnO promotes electrons from the valence band to the conduction band, leaving holes in the valence band [42]. The holes migrate from the valence band to deep levels and recombination occurs between electrons from either the conduction band or shallow donor levels and trapped holes on deep levels [43]. Basically, the PL of ZnO is related to the presence of holes in the valence band. Room temperature PL spectra of the GZO thin films measured using Xenon lamp of 325 nm as excitation source. The PL emission spectra of as deposited, air annealed and oxygen annealed GZO films with different thickness are shown in Fig. 8. The PL emission spectra of as deposited GZO films are very broad. All the films exhibited similar PL peaks and PL peak position is not altered with film thickness. The PL spectrum of as deposited GZO film with a thickness of 350 nm is deconvoluted (Gaussian deconvolution) into four bands to explain the PL mechanism in GZO films. The deconvoluted bands of as deposited GZO films are 419 nm (2.96 eV), 452 nm (2.74 eV), 491 nm (2.52 eV) and 530 nm (2.34 eV). These results are different from the earlier reports of GZO thin films [44–46]. Generally, oxygen vacancy (V_O) and interstitial zinc (Zn_i) are donors, and zinc vacancy (V_{Zn}), interstitial oxygen (O_i) and antisite oxygen (O_{Zn}) are acceptor in ZnO. These are various intrinsic defect centers in ZnO. It is well understood that PL spectra depend on the stoichiometry and the microstructure of the films. ZnO is nonstoichiometric oxide containing oxygen vacancy (V_O) and interstitial zinc species. These defects might have been formed when the zinc acetate was transformed

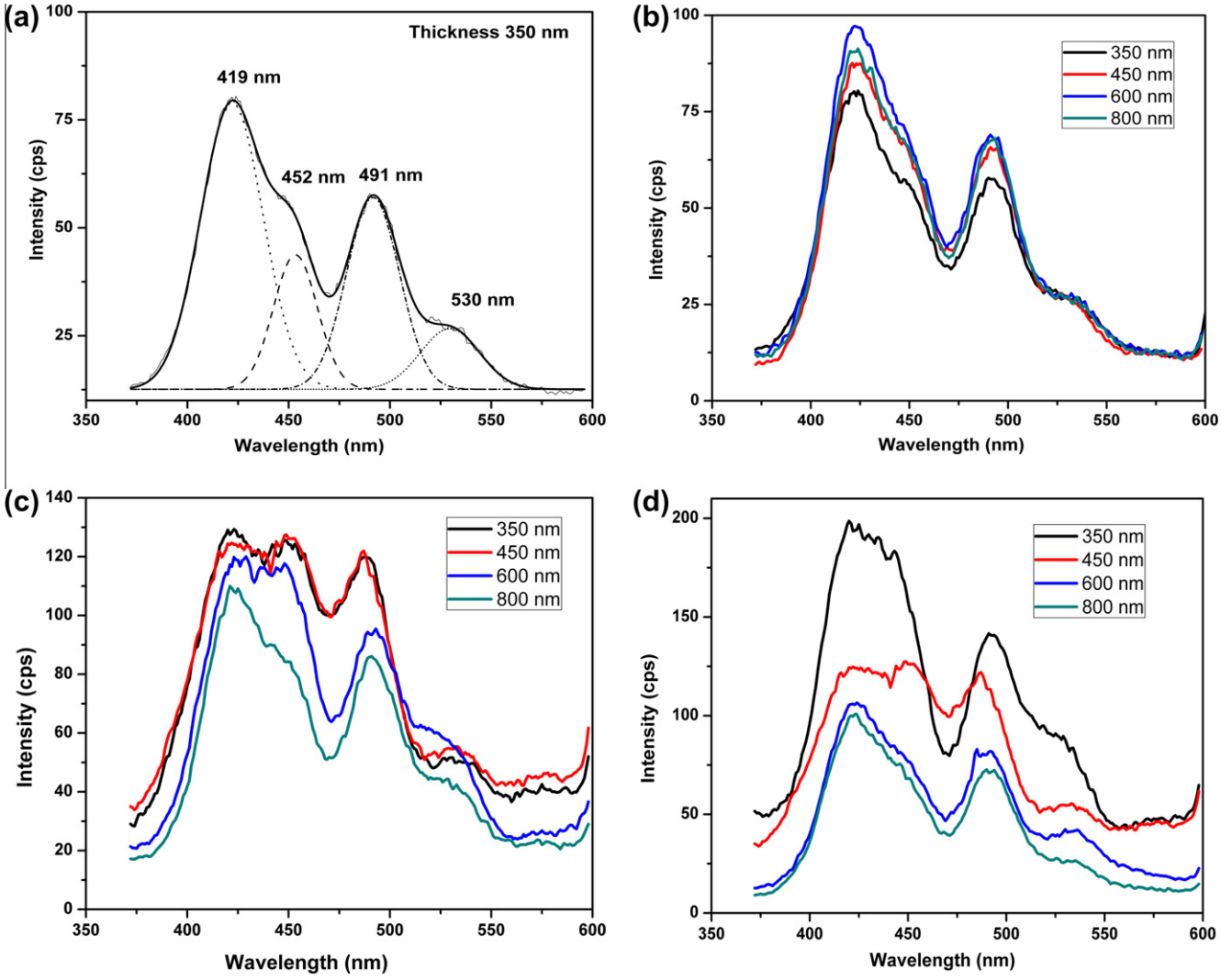

Fig. 8. PL emission spectra of GZO films (a) as deposited film with thickness 350 nm and dashed lines indicates the Gaussian deconvolution components (b) with different thickness (c) air annealed (d) oxygen annealed.

into ZnO in the spray pyrolysis process. The oxygen vacancy (V_O) might have been generated due to incomplete oxidation because of the rapid evaporation–oxidation that occurs in spray pyrolysis process.

The violet emission peak at 419 nm (2.96 eV) is probably due to radiative defects related to the interface traps existing at the grain boundaries [47]. This radiation transition occurs between these levels and valence band. This may be attributed to the large grain boundaries with non uniform grain sizes of as deposited GZO films. This argument is supported by AFM studies. The peak at 452 nm (2.72 eV) is blue emission, which originates from the defect emission of oxygen vacancies [48] and it is close to previously reported value of 2.66 eV [27]. The electronic transition for blue emission most likely occurs from the donor level of Zn interstitial to acceptor energy level of Zn vacancy. According to Sun et al. [49], the energy interval from the donor level of Zn interstitial to acceptor level of Zn vacancies is about 2.6 eV, which is close to the value of 2.72 eV for the blue emission in this study. There is a strong and broad green emission band centered at 491 nm (2.52 eV), which may have originated from the commonly assumed recombination of the photoexcited holes with the electrons occupying the singly ionized oxygen vacancies [50,51].

In general, the ZnO films with wurtzite structure contain large voids which can easily accommodate interstitial atoms. Consequently, it is impossible to prepare pure crystals (without voids or structural defects). Also, when these crystals are heated, they tend to lose oxygen [51]. The oxygen vacancies are generated due to the high surface energy obtained by annealing process at high temperature and the large lattice mismatch between film and substrate [51,52]. The changes in PL spectrum of GZO films due to annealing in air and oxygen are important in analyzing the optical quality of GZO. The PL peaks of annealed films in both atmospheres showed broad emission peaks in violet and blue-green spectral region. The intensity of the emission peaks found was to enhance with annealing. In the case of annealed GZO films, irrespective of the annealing atmosphere the intensity of the violet and blue emission is much higher compared to other two emissions. This may be due to increasing the Zn_i and V_O in GZO films. During annealing, it is possible for the coexistence of zinc vacancies (V_{Zn}) and zinc interstitials (Zn_i) in the films [52,53]. The deep-level blue luminescence can be correlated to the electronic transition from energy level of zinc interstitial (Zn_i) to that of zinc vacancy (V_{Zn}) (i.e. from near conduction-band edge to deep acceptor level) [53,54]. After annealing it is found that the blue-green emission decreases with the increase of film thickness of GZO. This may be attributed to the reduction in concentration of surface defects in GZO films with the increase of film thickness. But the PL emission spectrum of annealed films with a thickness 800 nm is similar to that of the as deposited GZO films. This means that films with smaller thickness are more affected by annealing process. This indicates that both the intrinsic shallow traps (V_{Zn}) and deep level vacancies (Z_{ni}, O_{Zn} and V_O) are affected [55] after the heat treatment. From the above discussion, it is confirmed that both the intrinsic traps and deep level vacancies are the most important factors that cause the broad visible emission from GZO thin films.

4. Conclusion

Polycrystalline GZO thin films were deposited by spray pyrolysis with various thicknesses. After deposition, the samples have been annealed at temperature 673 K in air and oxygen. The optical, electrical, and structural characteristics of the GZO films have been analyzed as a function of the film thickness and the annealing atmosphere. All these parameters decrease as the film thickness increases, whereas the mean crystalline size and the mobility increases as the film thickness grow up. All films were polycrystalline with a wurtzite phase, and exhibited a (002) preferential orientation almost irrespective of either the annealing atmosphere or thickness. The AFM images envisage a clear influence of the film thickness and annealing atmosphere on the surface morphology. The transmission in the UV region decreased obviously with the increase of film thickness. The band gap dependence on the film thickness and annealing atmosphere was associated with the shrinkage effect. From the PL studies, it was confirmed that both the intrinsic traps and deep level vacancies were the most important factors that cause the broad visible emission from GZO thin films.

Acknowledgements

Authors are grateful to Dr. V. Ganesan and Dr. S.R. Barman for extending AFM and XPS facilities for carrying out this work at UGC-CSIR Consortium for Scientific Research, Indore, India. T.P. Rao gratefully acknowledges the FCT, Portugal for providing Post-doctoral Fellowship.

References

[1] B. Lin, Z. Fu, Y. Jia, Appl. Phys. Lett. 79 (2001) 943.
[2] Shuang Liang, Xiaofang Bi, J.Appl. Phys. 104 (2008) 113533-1–113533-5.
[3] N. Jun-ichi, M. Konagai, K.Okada, T. Ito, T. Miyata, T. Minami, Thin Solid Films 518 (2010) 2937–2940.
[4] J. Zhong, S. Muthukumar, Y. Chen, Y. Lu, H.M. Ng, W. Jiang, E.L. Garfunkel, Appl. Phys. Lett. 83 (2003) 3401.
[5] B.E. Sernelius, K.F. Berggren, Z.C. Jin, I. Hamberg, C.G. Granqvist, Phys. Rev. B 37 (1988) 10244–10248.
[6] H. Fujiwara, M. Kondo, Phys. Rev. B 71 (2005) 075109–1 – 075109-10.
[7] T. Minami, H. Sato, H. Nanto, S. Takata, Jpn. J. Appl. Phys. 24 (1985) L781–L784.
[8] S. Takata, T. Minami, H. Nanto, Thin Solid Films 135 (1986) 183–187.
[9] H. Nanto, T. Minami, S. Orito, S. Takata, J. Appl. Phys. 63 (1988) 2711–2716.
[10] T. Minami, K. Oohashi, S. Takata, Thin Solid Films 193/194 (1990) 721–729.
[11] T. Minami, T. Miyata, T. Yamamoto, J. Vac. Sci. Technol. 17 (1999) 1822–1826.
[12] J.F. Chang, W.C. Lin, M.H. Hon, Appl. Surf. Sci. 252 (2005) 1561–1573.
[13] B. Bayraktaroglu, K. Leedy, R. Bedford, Appl. Phys. Lett. 93 (2008) 022104.
[14] V. Assuncao, E. Fortunato, A. Marques, A. Goncalves, I. Ferreira, H. Aguas, R. Martins, Thin Solid Films 442 (2003) 102–106.
[15] A. Van der Drift, Philips Res. Rep. 22 (1967) 267–288.
[16] N. Fujimura, T. Nishihara, S. Goto, et al., J. Cryst. Growth 130 (1993) 269–279.
[17] A. Kuroyanagi, J. Appl. Phys. 72 (1989) 5492.
[18] T. Prasada Rao, M.C. Santhoshkumar, Appl. Surf. Sci. 255 (2009) 4579–4584.
[19] J.F. Chang, C.C. Shen, M.H. Hon, Ceram. Int. 29 (2003) 245–250.
[20] M.K. Puchet, P.Y. Timbrell, R.N. Lamb, J. Vac.Sci. Technol. A 14 (1996) 2220–2230.
[21] X. Yu, J. Ma, F. Ji, Y. Wang, C. Cheng, H. Ma, Appl. Surf. Sci. 245 (2005) 310–315.
[22] J.F. Chang, W.C. Lin, M.H. Hon, Appl. Surf. Sci. 183 (2001) 18–25.
[23] M.N. Islam, T.B. Ghosh, K.L. Chopra, H.N. Acharya, Thin Solid Films 280 (1996) 20–25.
[24] G.E. Hammer, R.M. Shermenski, J. Vac. Sci. Technol. A 1 (1983) 1026–1028.
[25] J.F. Moulder, W.F. Stickel, P.E. Sobol, K.D. Bomben, Handbook of X-ray Photoelectron Spectroscopy: A Reference Book of Standard Spectra for Identification and Interpretation of XPS Data, Eden Prairie, MN, Physical Electronics, 1995.
[26] M. Chen, X. Wang, Y.H. Yu, Z.L. Pei, X.D. Bai, C. Sun, R.F. Huang, L.S. Wen, Appl. Surf. Sci. 158 (2000) 134–140.
[27] X.Q. Wei, B.Y. Man, M. Liu, C.S. Xue, H.Z. Zhuang, C. Yang, Phys. B Condens. Matter 388 (2007) 145–152.
[28] M.delaL. Olvera, H.G. mez, A. Maldonado, Sol. Energ. Mat. Sol. C. 91 (2007) 1449–1453.
[29] G.F. Neumark, Mater. Sci. Eng. R21 (1997) 1–46.
[30] S.S. Lin, J.L. Huang, P.S. ajgalik, Surf. Coat. Technol. 185 (2004) 254–263.
[31] T.L. Tansley, D.F. Neely, Thin Solid Films 121 (1984) 95–107.
[32] K.L Chopra, Thin Film Phenomena, McGraw-Hill, New York, 1969.
[33] D. Jiles, Introduction to the Electronic Properties of Materials, Chapman and Hall, New York, 1994.
[34] S.S. Lin, J.L. Huang, Surf. Coat. Technol. 185 (2004) 222–227.
[35] A.N. Banerjee, C.K. Ghosh, K.K. Chattopadhyay, H. Minoura, A.K. Sarkar, A. Akiba, A. Kamiya, T. Endo, Thin Solid Films 496 (2006) 112–116.
[36] H.P. He, F. Zhuge, Z.Z. Ye, L.P. Zhu, F.Z. Wang, B.H. Zhao, J. Appl. Phys. 99 (2006) 023503-1–023503-5.
[37] M. Suchea, S. Christoulakis, N. Katsarakis, T. Kitsopoulos, G. Kiriakidis, Thin Solid Films 515 (2007) 6562–6566.
[38] M. Bouderbala, S. Hamzaoui, M. Adnane, T. Sahraoui, M. Zerdali, Thin Solid Films 517 (2009) 572–1576.

[39] M.A.L. Lopez, A. Maldonado, R.C. Perez, G.T. Delgado, M.delaL. Olvera, Sol. Energ. Mat. Sol. C. 90 (2006) 2362–2376.
[40] A.P. Roth, J.B. Webb, D.F. Williams, Phys. Rev. B 25 (1982) 7836–7839.
[41] Q.B. Ma, Z.Z. Ye, H.P. He, L.P. Zhu, J.Y. Huang, Y.Z. Zhang, B.H. Zhao, Scr Mater 58 (2008) 21–24.
[42] K. Bouzid, A. Djelloul, N. Bouzid, J. Bougdira. Phys. Stat. Sol (a). 206 (2009) 06–115.
[43] D.C. Reynolds, D.C. Look, B. Jogai, J.E. Van Nostrand, R. Jones, J. Jenny, Solid State Commun. 106 (1998) 701–704.
[44] P.K. Nayak, J. Yang, J. Kim, S. Chung, J. Jeong, C. Lee, Y. Hong, J. Phys. D Appl. Phys. 41 (2008) 135404.
[45] J.A. Sans, A. Segura, J.F.S. Royo, V. Barber, M.A.H. Fenollosa, B. Marib, Superlattices Microstruct. 39 (2006) 282–290.
[46] L. Zhu, J. Li, Z. Ye, H. He, X. Chen, B. zhao, Opt. Mater. 31 (2008) 237–240.
[47] B.J. Jin, S. Im, S.Y. Lee, Thin Solid Films 366 (2000) 07–110.
[48] Y.H. Tong, Y.C. Liu, S.X. Lu, L. Dong, S.J. Chen, Z.Y. Xiao, J. Sol-Gel. Sci. Technol. 30 (2004) 157–161.
[49] Y. M. Sun, Ph.D. Thesis, University of Science and Technology of China, 2000.
[50] K. Vanheusden, W.L. Warren, C.H. Seager, D.R. Tallant, J.A. Voigt, B.E. Gnade, J. Appl. Phys. 79 (1996) 7983–7990.
[51] Leonid V. Azaroff, Introduction to solids, McGraw-Hill, New York, 1960.
[52] H.S. Kang, J.S. Kang, J.W. Kim, S.Y. Lee, J. Appl. Phys. 95 (2004) 1246–1250.
[53] P.S. Xu, Y.M. Sun, C.S. Shi, F.Q. Xu, H.B. Pan, Nucl. Instr. Meth. B 199 (2003) 286–290.
[54] A. Ghosh, R.N.P. Choudhary, Phys. Stat. Sol. (a) 206 (2009) 535–539.
[55] S.A. Studenikin, M. Cocivera, J. Appl. Phys. 91 (2002) 5060–5065.